Supporting Information

Tagged Simulation Regions

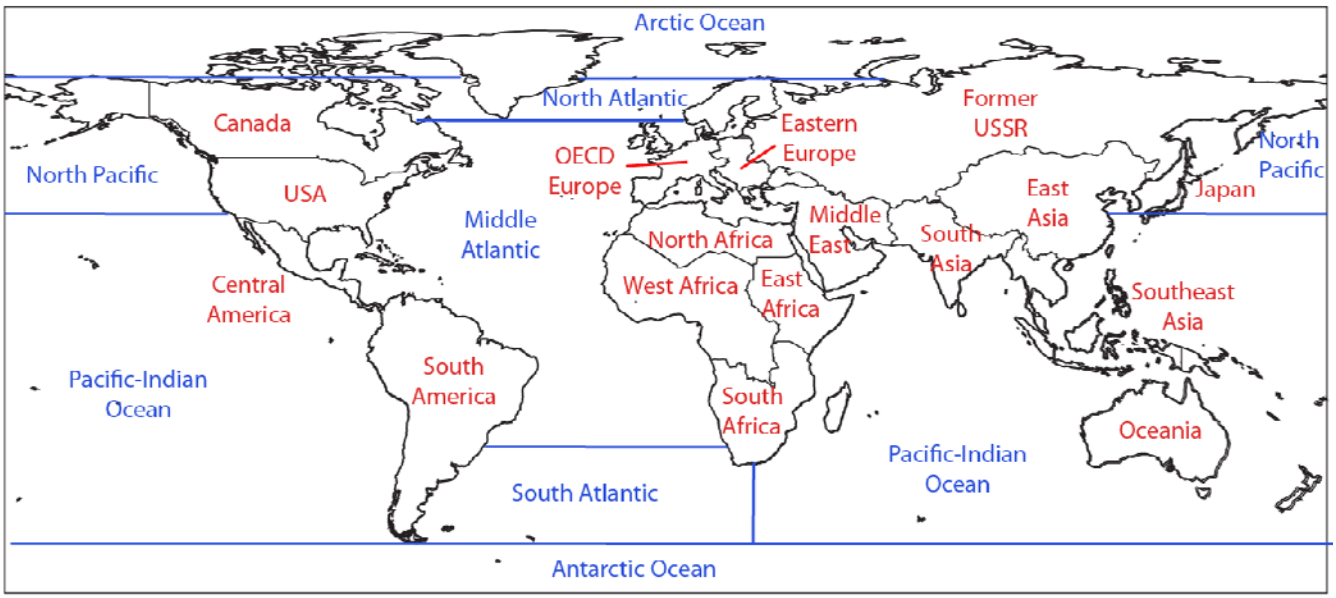

SI Figure 1 Definition of source and receptor regions: 17 anthropogenic emissions regions are from IMAGE 2.2 and are used in Streets et al. (1); 7 ocean regions from Soerensen et al. (2).

Emissions Scenarios

Our simulations are based on the mercury emissions projections by Streets et al. (1) for four IPCC scenarios of economic and technologic development (A1B, A2, B1, B2). Global economic growth is expected in all scenarios, though at a faster pace in the A scenarios. Globalization in the A1B and B1 scenarios is associated with widely distributed economic growth. Developmental paths diverge more in the A2 and B2 scenarios, with relatively more growth in already advanced industrialized countries. In all scenarios, coal-fired power production, especially in Asia, drives the largest changes in mercury emissions. In the A scenarios, industrialized countries aggressively use emissions control technology but implementation is variable among developing countries and removal efficiency is capped at the present-day level (40%). In the B scenarios, emissions controls are extended to more regions, and technology improves to 52-70% removal efficiency.

Streets et al. (1) use flue-gas desulfurization (FGD) as a proxy for all mercury emission control technologies, and adjust assumptions about capture efficiency and technological penetration in developing countries for each scenario. Even without regulation targeted specifically at mercury emission, FGD may be installed to limit emission of other air pollutants and will capture mercury as a co-benefit.

SI Table 1 (next page) Present and future (2050) global mercury emissions and deposition and fraction of deposition from regional sources (f_d). Emissions are from Streets et al. (1), modified to include emissions from fuel combustion and industrial processes only, i.e. does not include biomass burning. Deposition is gross downward flux and is greater than the sum of anthropogenic and non-varying natural and historical emissions (6100 Mg/y) due to recycling in the surface ocean, vegetation, and snow reservoirs. Annual emissions and deposition are rounded to the nearest hundred Mg. We calculate f_d as the fraction of total deposition in a model grid box that originates from anthropogenic sources in the same world region.

Scenario	Description	Anthropogenic Emissions (Mg a^{-1})	Gross Total Deposition (Mg a^{-1})	f_d (%) Gross	f_d (%) Net
Present-day	Sectors: Industrial processes 53% Power plant combustion 24% Residential/industrial fuel 23% Speciation: 57% $Hg^{0,}$ 37% Hg^{II}, 6% Hg^{P} 40% removal efficiency Largest anthro: East Asia 51%, USA 7%	1900	9600	10.4	9.3
2050 A1B	Sectors: Industrial processes 24% Power plant combustion 56% Residential/industrial fuel 20% Speciation: 40% Hg^{0}, 55% Hg^{II}, 5% Hg^{P} 40% removal efficiency Largest anthro: East Asia 33%, South Asia 27%	4300	11600	16.0	14.4
2050 A2	Sectors: Industrial processes 33% Power plant combustion 38% Residential/industrial fuel 29% Speciation: 45% Hg^{0}, 47% Hg^{II}, 8% Hg^{P} 40% removal efficiency Largest anthro: East Asia 41%, South Asia 14%	3400	12000	15.6	14.2
2050 B1	Sectors: Industrial processes 31% Power plant combustion 49% Residential/industrial fuel 20% Speciation: 45% Hg^{0}, 50% Hg^{II}, 5% Hg^{P} Removal efficiency: 70% developed regions 52% developing regions Largest anthro.: East Asia 31%, South Asia 21%	1900	9700	11.9	10.9
2050 B2	Sectors: Industrial processes 29% Power plant combustion 51% Residential/industrial fuel 20% Speciation: 43% Hg^{0}, 52% Hg^{II}, 5% Hg^{P} Removal efficiency: 70% developed regions 52% developing regions Largest anthro: East Asia 34%, South Asia 22%	2200	10300	12.7	11.6

[a]From Streets et al. (1)

Ocean Evasion

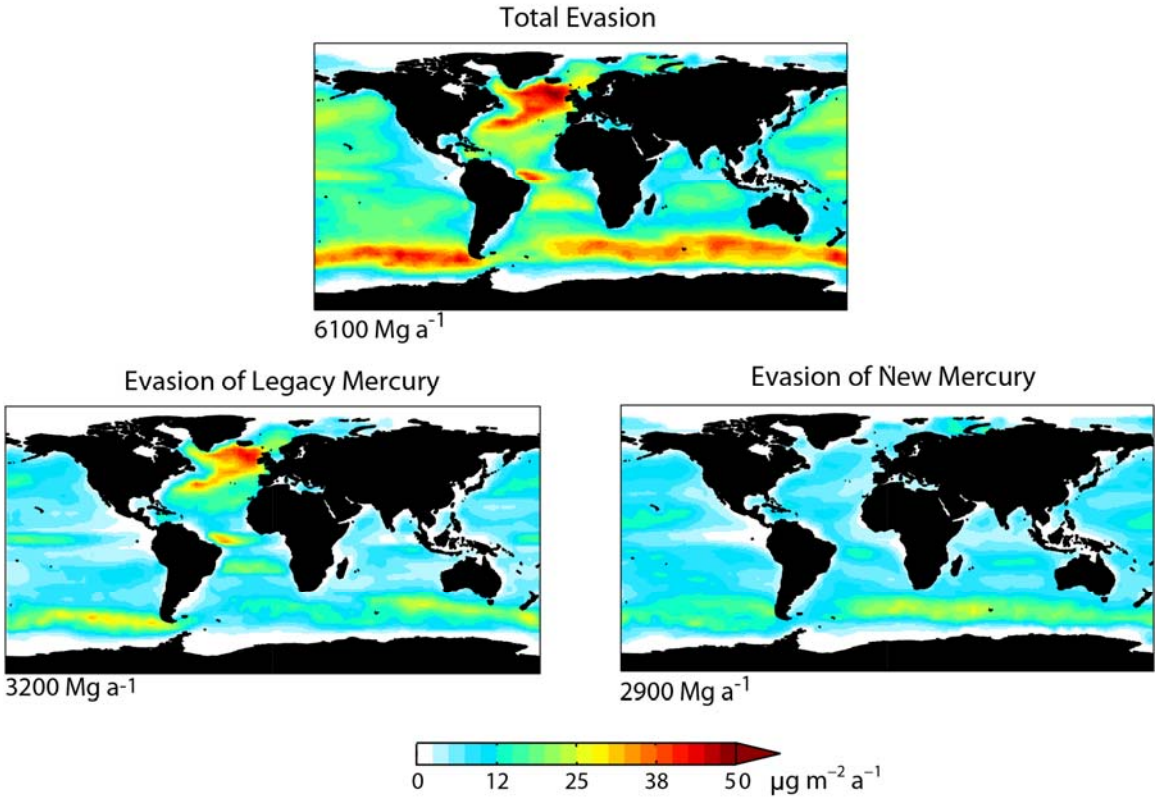

SI Figure 2 Gross evasion of mercury from the surface ocean to atmosphere divided into components from fast re-emission of recently deposited mercury and upwelling of legacy mercury from subsurface waters.

Net Deposition for All Scenarios

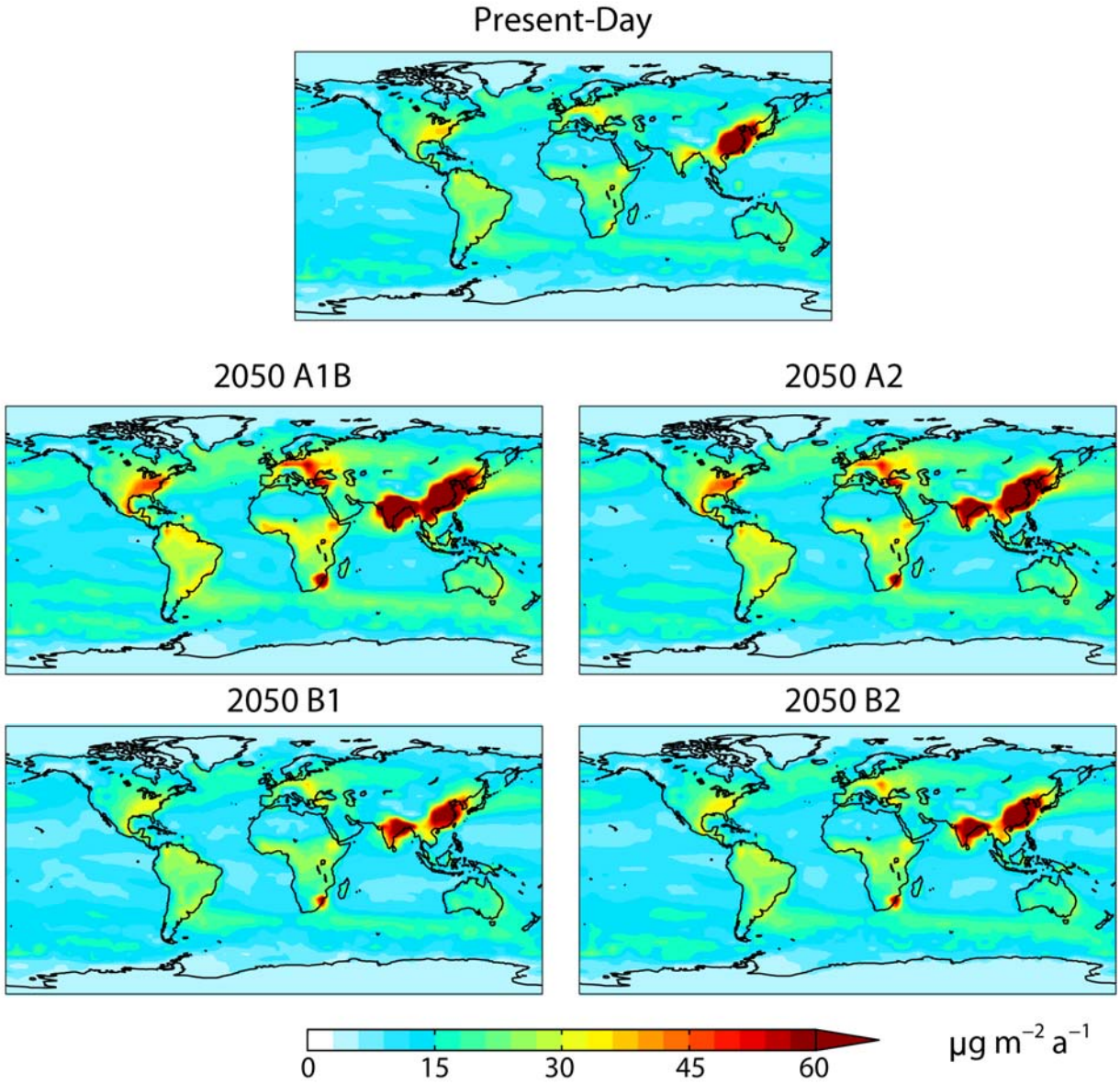

SI Figure 3 Global net deposition of mercury for the present-day and four IPCC scenarios.

Fraction of Deposition from Domestic Sources

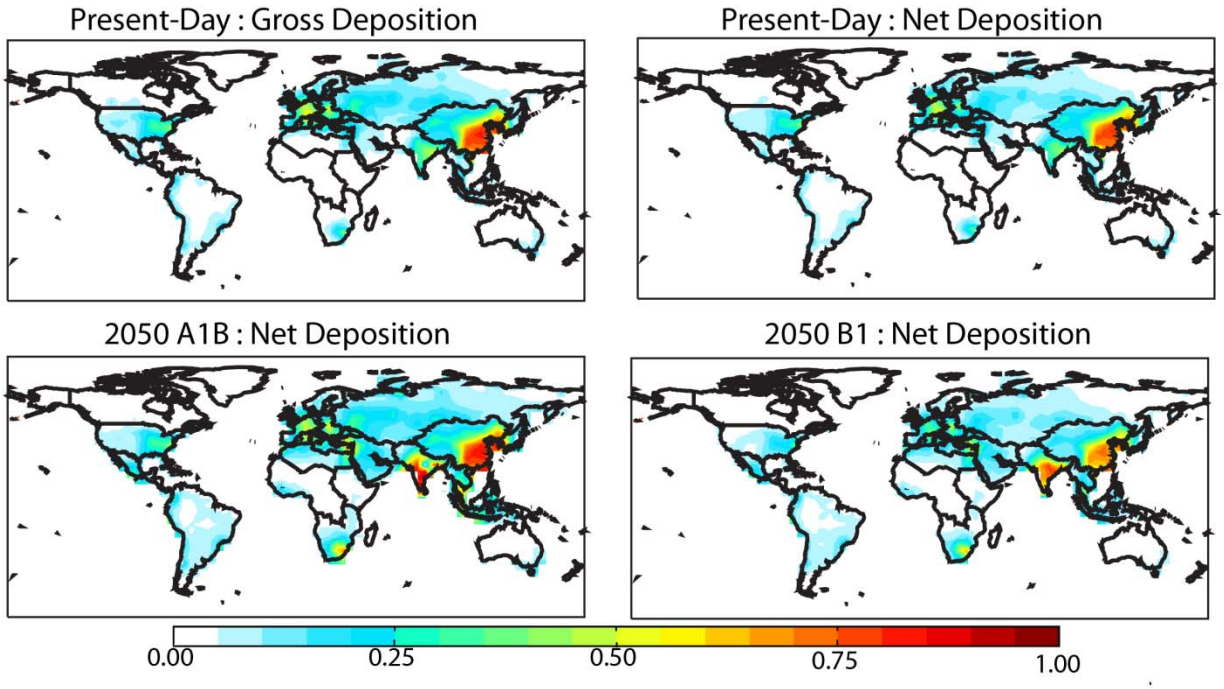

SI Figure 4 Fraction f_d of deposited mercury originating from anthropogenic sources within the same continental region indicated by heavy black lines. **Top panel:** F_d for gross and net deposition in the present-day. **Bottom panel:** F_d for net deposition in the 2050 A1B and B1 scenarios.

Influence Functions

We define the source-receptor influence function I_{ij} for mercury deposition as:

$$I_{ij} = \frac{D_{ij}}{E_i} \quad (1)$$

where D_{ij} is the net deposition flux to receptor region j from emissions in region i, and E_i is the total emission rate for region i. Examining influence functions enables us to evaluate where, gram-for-gram, emissions reductions would be most effective to reduce deposition to a given region.

The effective lifetime of Hg^0 taking into account reduction of Hg^{II} and recycling of deposited mercury is 9 months, still shorter than the timescale for interhemispheric exchange (~1 year (3)), meaning that Hg^0 is not globally well-mixed in the atmosphere. Previous studies have used observations of atmospheric variability, including the interhemispheric gradient, to estimate an Hg^0 lifetime of 0.5-2 years (4-6). This variability is well reproduced by GEOS-Chem, lending support to our lifetime estimates (7).

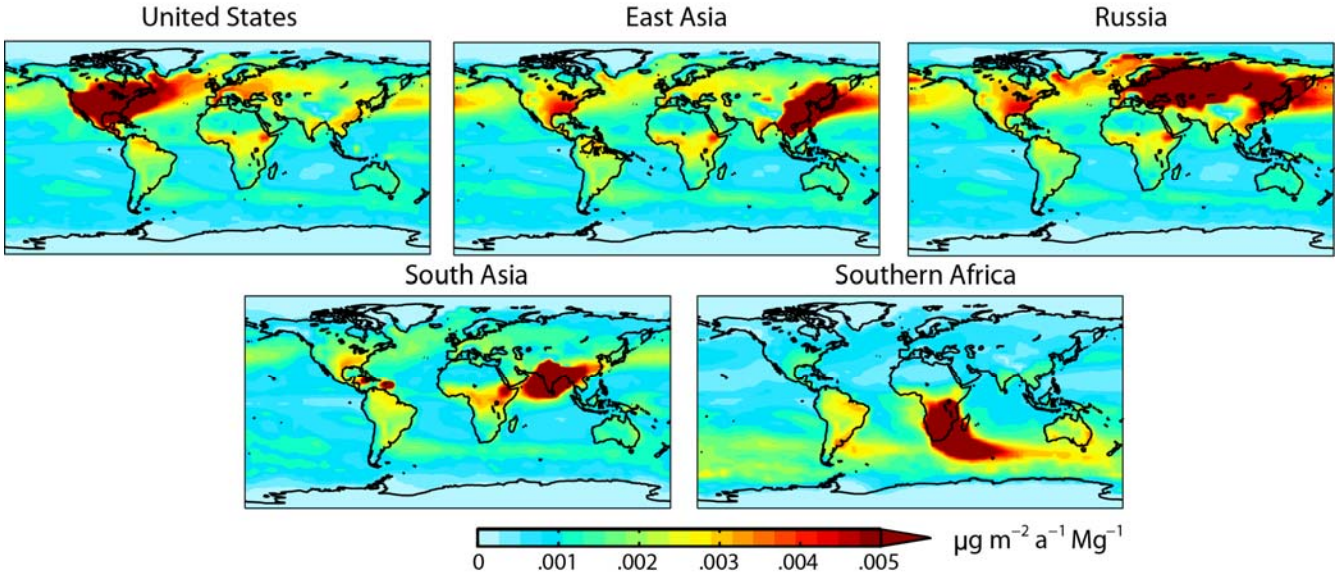

SI Figure 5 Influence functions for the present day for selected source regions: United States, East Asia, Russia, South Asia, and Southern Africa.

Regional Exporters and Importers of Anthropogenic Mercury

The ratio of anthropogenic mercury exported from a region and deposited elsewhere to the imported mercury deposited within the region from all external sources (R_E) is highly variable across regions and scenarios (Figure 6). In the present-day, East Asia has the greatest ratio of exports to imports (R_E=6) as expected due to its majority share of global anthropogenic emissions. The most importing regions (R_E < 0.2) are generally those which have the lowest emissions: West Africa, Canada, and Oceania. In the 2050 simulations, rapidly developing regions, such as South Asia, Central America, the Middle East, and Africa become more exporting in all scenarios, though may remain net importers. East Asia, Western Europe, Canada, and Oceania trend toward less exporting as the majority of any emissions increases are as Hg^{II} and deposit locally. The United States becomes more exporting in the A scenarios and more importing in the B scenarios, but remains a net importer in all future scenarios.

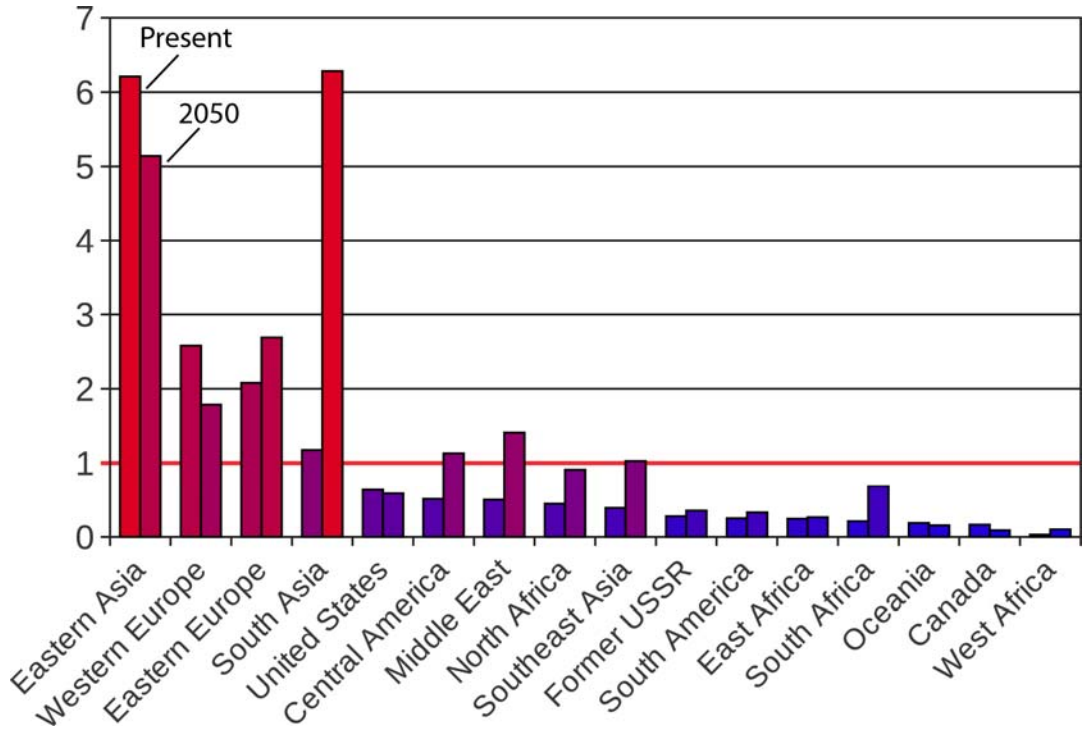

SI Figure 6 Ratio of exported to imported mercury deposition (R_E) by region for the present-day (first column) and average across all 2050 scenarios (second column). Red indicates regions that are net exporters (R_E>1) and blue indicates net importers (R_E<1).

Linear Regression Analysis

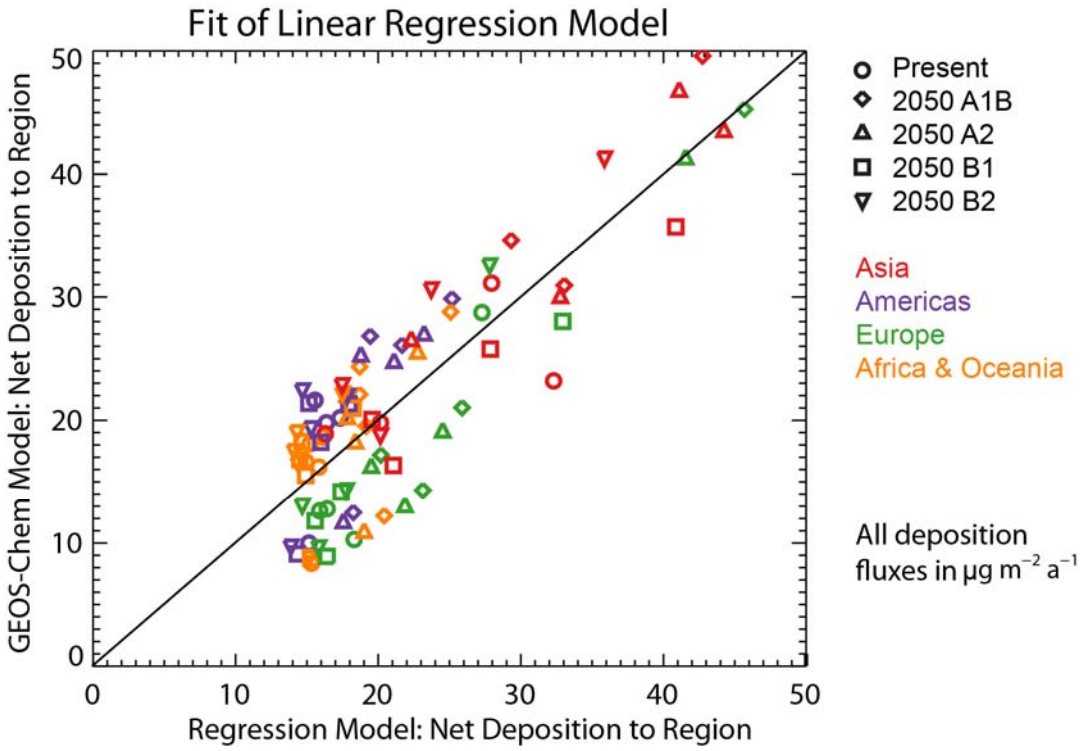

SI Figure 7 Fit of linear regression model for quick estimation of mean regional mercury deposition compared to deposition from the full atmosphere-land-ocean model. Regression model formula:

$$D_R = 0.39\, E_{R\,Hg}^{II} + 0.74\, E_{G\,Hg}^{0} + 10 \qquad (2)$$

All values in μg m^{-2} a^{-1}.

Model Sensitivity Analysis

The GEOS-Chem biogeochemical mercury model has been extensively evaluated with all available atmospheric and oceanic measurements in other studies (2,7-8). Here we evaluated the model's sensitivity to atmospheric redox reactions by comparing two alternate simulations to the base runs with Br as the major atmospheric oxidant and slow in-cloud reduction.

Total regional deposition in the simulation without in-cloud reduction differs by no more than 12% relative to the base simulation. Local differences may be up to 25%, with less deposition in remote areas of Antarctica and the Sahara, for example, and more deposition downwind of large Asian sources in Japan and Indonesia.

We found that modeled deposition using OH and O_3 as the major oxidant of Hg^0 instead of Br atoms does not change total deposition to any mid-latitude region by more than 12%. Above 60^o latitude, cold temperatures and the comparatively greater proportion of Br atoms, especially during springtime atmospheric mercury depletion events, enhance oxidation and deposition up to 78% compared to the OH/O_3 simulation. Net deposition in the OH/O_3 compared to the base simulation is 23% to the Arctic Ocean and72% less across Antarctica. At low latitudes, such as in northern Africa, southern Asia, and the Middle East, greater oxidation of Hg^0 in the OH/O_3 simulation increases modeled regional deposition up to 59% relative to the Br simulation. Our results are consistent with those from an inter-comparison of six mercury models for the Task Force on Hemispheric Transport of Air Pollution (HTAP), which found that modeled deposition was comparable in many regions globally but that polar regions are especially sensitive to model chemistry and transport (9).

Despite these differences in deposition magnitude in polar regions and at low latitudes, the composition of sources across the three sensitivity tests remains essentially unchanged (±2% and ±3%, respectively). This occurs because source contributions to the hemispheric atmospheric background dictate their relative abundance in deposition to remote regions rather than atmospheric oxidation. These results confirm that uncertainty in the magnitude of deposition in certain regions globally does not preclude an analysis of source contributions to deposition.

The extent to which scientific uncertainties affect our ability to reliably simulate deposition close to power plant and industrial sources in the eastern United States is of special concern to policy-makers. From our sensitivity analysis, we find that mean f_d for the eastern United States is 0.23, 0.25, or 0.20 for the base, no reduction, and OH/ O_3 oxidation cases, respectively. The relatively constrained range of modeled f_d bolsters the conclusion that both global and regional sources are important to deposition for the eastern U.S. A greater uncertainty is the proposed in-plume reduction of HgII. Observational studies have estimated that 10-90% of emitted Hg^{II} is reduced to Hg^0 over a period of >1 to 5 hours (10-12). This conversion would reduce the component of local deposition near sources, but the mechanism is currently unknown.

In the heavily impacted Ohio River Valley region, U.S. anthropogenic sources dominate the total changes in deposition in the 2050 scenarios. Anthropogenic deposition in this region decreases by 32% in the strictest emissions scenario considered here, but could decline even further if sorbent technologies, not currently commercially available, were implemented. Streets et al. (1) found that U.S. mercury emissions from power plants increased from 1996 to 2006. In the absence of regulation, continued growth in coal-fired power plants over the coming decades would likely increase U.S. mercury emissions and local deposition.

SI References

(1) Streets, D. G.; Zhang, Q.; Wu, Y. Projections of Global Mercury Emissions in 2050. *Environmental Science & Technology* **2009**, *43* (8), 2983.

(2) Soerensen, A. L.; Sunderland, E. M.; Holmes, C. D.; Jacob, D. J.; Yantosca, R. M.; Skov, H.; Christensen, J. H.; Strode, S. A.; Mason, R. P. An Improved Global Model for Air-Sea Exchange of Mercury: High Concentrations over the North Atlantic. *Environmental Science & Technology* **2010**, *44* (22), 8574.

(3) Jacob, D. J.; Prather, M. J.; Wofsy, S. C.; McElroy, M. B. Atmospheric distribution of Kr-85 simulated with a general-circulation model. *Journal of Geophysical Research-Atmospheres* **1987**, *92* (D6), 6614.

(4) Slemr, F.; Schuster, G.; Seiler, W. Distribution, speciation, and budget of atmospheric mercury. *J. Atmos. Chem.* **1985**, *3* (4), 407.

(5) Lin, C. J.; Pehkonen, S. O. The chemistry of atmospheric mercury: a review. *Atmospheric Environment* **1999**, *33* (13), 2067.

(6) Lindberg, S.; Bullock, R.; Ebinghaus, R.; Engstrom, D.; Feng, X. B.; Fitzgerald, W.; Pirrone, N.; Prestbo, E.; Seigneur, C. A synthesis of progress and uncertainties in attributing the sources of mercury in deposition. *Ambio* **2007**, *36* (1), 19.

(7) Holmes, C. D.; Jacob, D. J.; Corbitt, E. S.; Mao, J.; Yang, X.; Talbot, R.; Slemr, R. Global atmospheric model for mercury including oxidation by bromine atoms. *Atmospheric Chemistry and Physics* **2010**, *10* (24), 12037.

(8) Selin, N. E.; Jacob, D. J.; Yantosca, R. M.; Strode, S.; Jaegle, L.; Sunderland, E. M. Global 3-D land-ocean-atmosphere model for mercury: present-day versus preindustrial cycles and anthropogenic enrichment factors for deposition. *Global Biogeochemical Cycles* **2008**, *22* (2), GB2011.

(9) Travnikov, O.; Lin, C.-J.; Dastoor, A.; Bullock, O. R.; Hedgecock, I. M.; Holmes, C. D.; Ilyin, I.; Jaegle, L.; Jun, G.; Pan, L.; Pongrueksa, P.; Ryzhkov, A.; Seigneur, C.; Skov, H. *Mercury: Global and Regional Modeling*, 2011.

(10) Lohman, K.; Seigneur, C.; Edgerton, E.; Jansen, J. Modeling mercury in power plant plumes. *Environmental Science & Technology* **2006**, *40* (12), 3848.

(11) Edgerton, E. S.; Hartsell, B. E.; Jansen, J. J. Mercury speciation in coal-fired power plant plumes observed at three surface sites in the southeastern US. *Environmental Science & Technology* **2006**, *40* (15), 4563.

(12) Ter Schur, A.; Caffrey, J.; Gustin, M.; Holmes, C.; Hynes, A.; Landing, B.; Landis, M.; Laudel, D.; Levin, L.; Nair, U.; Jansen, J.; Ryan, J.; Walters, J.; Schauer, J.; Volkamer, R.; Waters, D.; Weiss-Penzias, P. An integrated approach to assess elevated mercury wet deposition and concentrations in the southeastern United States. *10th International Conference on Mercury as a Global Pollutant* Halifax, NS, Canada, 2011.